Suppressing falling film instabilities by Marangoni forces

Evgeny A. Demekhin, Serafim Kalliadasis, and Manuel G. Velarde

Citation: Physics of Fluids **18**, 042111 (2006); doi: 10.1063/1.2196450
View online: http://dx.doi.org/10.1063/1.2196450
View Table of Contents: http://scitation.aip.org/content/aip/journal/pof2/18/4?ver=pdfcov
Published by the AIP Publishing

Suppressing falling film instabilities by Marangoni forces

Evgeny A. Demekhin
Department of Applied Mathematics, Kuban State Technological University, Krasnodar 350072, Russia

Serafim Kalliadasis
Department of Chemical Engineering, Imperial College London, London SW7 2AZ, United Kingdom

Manuel G. Velarde
Instituto Pluridisciplinar, Universidad Complutense, Paseo Juan XXIII, No. 1, 28040 Madrid, Spain

(Received 14 April 2005; accepted 15 March 2006; published online 28 April 2006)

The linear stability of a thin liquid layer falling down an inclined wall heated by a downstream linearly increasing temperature distribution is investigated. It is shown that hydrodynamic and Marangoni instabilities yield two types of transverse instabilities: long surface waves and convective rolls, and longitudinal convective rolls, much like in the case of a uniformly heated wall. However, in contrast to the problem of a uniformly heated wall, where the thermocapillary forces have a destabilizing influence on all instability modes, here they can either destabilize or stabilize the flow. For liquids with sufficiently large Prandtl numbers, increasing the temperature gradient first destabilizes the flow and then stabilizes it. On the other hand, for small Prandtl numbers, increasing the temperature gradient leads to a monotonic stabilization of all instability modes.
 [DOI: 10.1063/1.2196450]

I. INTRODUCTION

The Marangoni effect induced by temperature or concentration gradients can cause fluid motion from a region of low surface tension to a region of large surface tension, even against gravitational forces.[1,2] The same thermocapillary stress is also responsible for a number of other phenomena such as "tears of wine or spirit"[3] when a thin film of a water-alcohol mixture loses the latter by evaporation, hence increasing its surface tension, and shows drop motion against gravity forces along the wall of a glass. Such flows are of interest in a number of practical applications, including partial condensers/film coolers, wetted wall columns, and gas diffusion electrodes. In all these applications, the film flow may exhibit a number of instabilities, e.g., there might be interfacial waves and related convected flows that are thought to be responsible for significant changes in heat/mass transfer and overall pressure drop.

The thermocapillary instability of a horizontal liquid layer heated uniformly from below was first examined by Pearson[4] and Scriven and Sternling.[5] Pearson obtained a short-wave thermocapillary mode, but he assumed a nondeformable free surface, even though he emphasized the role of surface tension. The exact conditions for which the Pearson result can be obtained were developed by Velarde *et al.*[6] and include small temperature gradients across the film and small film thicknesses. Scriven and Sternling, on the other hand, allowed the free surface to deform, but discarded gravity. Hence, there was no hydrostatic contribution at the deformable interface. They obtained a long-wave thermocapillary mode, but the absence of gravity was shown to yield no threshold. This issue was analyzed in detail by Velarde *et al.*[6]

Smith[7] extended Pearson's and the Scriven and Sternling theories by incorporating gravity in the boundary conditions describing a deformable interface between two adjacent phases with a given finite depth and bounded by perfectly conducting surfaces. The same problem was also considered by Goussis and Kelly,[8] while Smith and Davis,[9,10] Davis,[11] and Shevtsova *et al.*[12] investigated the instability of a horizontal liquid layer heated from below by a constant temperature gradient. For a detailed review of the Marangoni instability of horizontal liquid layers heated from below, the reader is referred to the studies by Velarde *et al.*,[6] Davis,[11] Colinet *et al.*,[13] and Velarde and Zeytounian.[14]

For a film falling down a uniformly heated plane, Goussis and Kelly[15] investigated the coupled Orr-Sommerfeld and linearized energy equations by means of asymptotic and numerical analyses. These authors demonstrated that in general there are three types of instabilities: (i) long-wave surface transverse instability. This is the classical Kapitza hydrodynamic mode of instability for an isothermal falling film due to inertia;[16] (ii) long-wave surface transverse modes driven by thermocapillary stresses; (iii) short-wave rolls, longitudinal or transverse, also driven by thermocapillary stresses. For these modes the deformation of the free surface is not important (dilation-compression waves).

The first two modes have been analyzed via a long-wave nonlinear analysis based on the lubrication approximation by Bankoff[17] and Joo *et al.*[18] A nonlinear analysis of these two modes was also performed more recently by Kalliadasis *et al.*[19] based on an integral-boundary-layer approximation of the Navier-Stokes and energy equations and associated boundary conditions. The same approximation was also utilized by Kalliadasis *et al.*[20] to analyze the transverse thermocapillary instability on the surface of a film heated from below by a local heat source. The integral-boundary-layer approximation model introduced in Ref. 19 is an extension of the integral-boundary-layer approximation developed by Shkadov[21,22] for isothermal falling films to include thermal

effects. Hence, the model suffers from the same limitations as the Shkadov model: it does not predict very accurately neutral and critical conditions and introduces an error, typically of the order of 20% for the critical Reynolds number for the onset of the instability compared to the exact value obtained from a direct Orr-Sommerfeld stability analysis of the full Navier-Stokes and energy equations. Moreover, the formulation in Ref. 19 neglected the second-order dissipative effects that are known to determine the amplitude of the front-running capillary waves in the case of isothermal flows.[23] These deficiencies have been recently corrected in Refs. 24–26 by developing a high-order weighted residual approach with polynomial test functions for both velocity and temperature fields.

Shkadov *et al.*[27] recently analyzed the linear stage of the instability of a falling film in the presence of surfactants by using an integral-boundary-layer approximation, while Trevelyan and Kalliadasis[28,29] performed a linear and nonlinear analysis of a falling film in the presence of exothermic chemical reactions by using both a long-wave expansion and an integral-boundary-layer approximation. In this case the Marangoni effect is induced by the heat released by the chemical reactions.

In this study we investigate the problem of film falling down a planar wall heated with a constant temperature gradient. The same problem was considered by Ludviksson and Lightfoot,[30] but these authors restricted their attention to a stability analysis in the spanwise direction only. The linear analysis of transverse surface waves on a falling film with a constant temperature gradient along the wall was recently considered by Miladinova *et al.*[31,32] using the lubrication approximation. The same authors also performed a nonlinear analysis of transverse surface waves based on the lubrication approximation.

Here we focus on the linear stage of the instability for the same problem. We perform a detailed and systematic analysis of the Orr-Sommerfeld and linearized energy equations via appropriate asymptotic and numerical methods. Unlike the previous studies, our investigation covers all possible types of instability, and, in fact, we demonstrate that the existence of a temperature gradient along the wall, rather than a constant temperature, causes the same kinds of instability with the uniformly heated case analyzed by Goussis and Kelly,[15] i.e., transverse surface waves, transverse rolls, and longitudinal rolls, albeit significantly altered. The differences with the uniformly heated case are primarily due to the fact that the base Nusselt flow solution now depends on the Marangoni number and such that thermocapillary stresses move liquid up against gravity (the temperature gradient is directed in the downstream direction). As a consequence, the temperature profile is no longer a linear function of the coordinate perpendicular to the wall, but it is given by a fourth-order polynomial whose coefficients depend strongly on the flow features.

II. FORMULATION

We consider a liquid film with density ρ, shear viscosity μ, and surface tension σ falling down an inclined plane $y=0$ with inclination angle θ with respect to the horizontal direction. Figure 1 sketches the flow situation. The film is heated from the wall side with a downward linearly increasing temperature distribution. This leads to a "cold" top and a "hot" bottom that induces an upstream-directed thermocapillary Marangoni stress on the free surface. Such a linear temperature distribution can be achieved by a metal block (the metal should be a good heat conductor, e.g., copper) placed below the substrate and heated from the downstream side. Let $y=h(x,z,t)$ denote the location of the interface with z the transverse direction. The ambient gas phase is air and its pressure without a loss of generality is taken to be zero as a reference value.

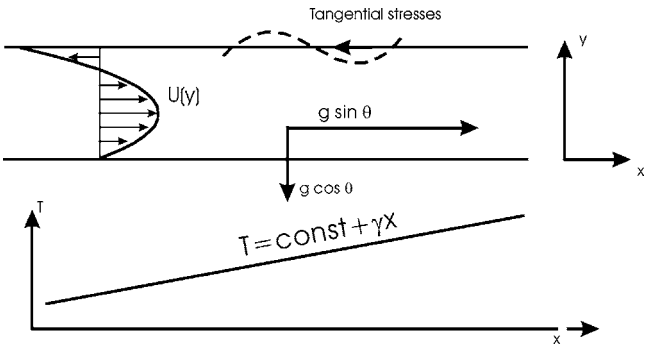

FIG. 1. Film falling down an inclined wall with inclination angle θ with respect to the horizontal direction. The film is heated from the wall side with a downward linearly increasing temperature distribution leading to a "cold" top and a "hot" bottom.

The governing equations are the Navier-Stokes, continuity, and energy equations,

$$\frac{\mathrm{D}\mathbf{v}}{\mathrm{D}t} = -\rho^{-1}\,\boldsymbol{\nabla} p + \nu\,\nabla^2\mathbf{v} + \mathbf{G}, \tag{1a}$$

$$\boldsymbol{\nabla}\cdot\mathbf{v} = 0, \tag{1b}$$

$$\frac{\mathrm{D}T}{\mathrm{D}t} = a\,\nabla^2 T, \tag{1c}$$

where $\mathrm{D}/\mathrm{D}t \equiv \partial/\partial t + \mathbf{v}\cdot\boldsymbol{\nabla}$ is the material derivative and $\boldsymbol{\nabla} \equiv (\partial/\partial x, \partial/\partial y, \partial/\partial z)$ is the gradient operator. Here $\mathbf{v} = (u,v,w)$ is the liquid velocity vector with components u, v, and w in the x, y, and z directions, respectively, and p and T are the pressure and temperature of the liquid, respectively; $\mathbf{G} = (g\sin\theta, -g\cos\theta, 0)$, $\nu = \mu/\rho$ and a are the body force, kinematic viscosity, and thermal diffusivity of the liquid, respectively. These equations are subject to the boundary conditions

$$-p + (\mathbf{P}\cdot\mathbf{n})\cdot\mathbf{n} = 2\sigma_0 K(h), \tag{2a}$$

$$(\mathbf{P}\cdot\mathbf{n})\cdot\boldsymbol{\tau}_\mathbf{i} = \boldsymbol{\nabla}_s\sigma\cdot\boldsymbol{\tau}_\mathbf{i}, \quad i = 1,2, \tag{2b}$$

$$\boldsymbol{\nabla}T\cdot\mathbf{n} = 0, \tag{2c}$$

$$v = \frac{\partial h}{\partial t} + \mathbf{v}\cdot\boldsymbol{\nabla}h \tag{2d}$$

at $y=h(x,z,t)$ and

$$\mathbf{v} = \mathbf{0}, \tag{3a}$$

$$T = \text{const} + \gamma x \tag{3b}$$

at $y=0$, where $\gamma(>0)$ denotes the constant temperature gradient imposed along the wall. Without loss of generality the arbitrary constant in (9) is set equal to zero.

Equation (2a) is the normal stress balance with σ_0 the surface tension at a reference temperature T_0, $\mathbf{P}=2\mu\mathbf{E}$ is the deviatoric stress tensor with $\mathbf{E}=(1/2)[\boldsymbol{\nabla}\mathbf{v}+(\boldsymbol{\nabla}\mathbf{v})^{\mathrm{t}}]$ the rate-of-strain tensor[33] and $K(h)=-(1/2)\boldsymbol{\nabla}\cdot\mathbf{n}$ the curvature of the interface[34] with $\mathbf{n}$ the outward unit normal to the interface defined from

$$\mathbf{n} = \frac{1}{n}(-h_x, 1, -h_z),$$

with $n=(1+h_x^2+h_z^2)^{1/2}$. Equations (2b) are the tangential stress balances with

$$\boldsymbol{\tau_1} = \frac{1}{\tau_1}(1, h_x, 0) \quad \text{and} \quad \boldsymbol{\tau_2} = \frac{1}{\tau_2}(0, h_z, 1),$$

unit vectors tangential to the interface with $\tau_1=(1+h_x^2)^{1/2}$ and $\tau_2=(1+h_z^2)^{1/2}$ the modulus of vectors $\boldsymbol{\tau_1}$ and $\boldsymbol{\tau_2}$, respectively; $\boldsymbol{\nabla}_s=(\mathbf{I}-\mathbf{nn})\cdot\boldsymbol{\nabla}$ is the surface gradient operator and $\boldsymbol{\tau_i}\cdot\boldsymbol{\nabla}_s\sigma = -(\kappa/\tau_i)(T_x+h_xT_y)|_{y=h}$, where κ is defined from the linear approximation for the surface tension

$$\sigma = \sigma_0 - \kappa(T - T_0), \quad \kappa > 0. \tag{4}$$

Equation (2c) is obtained with the assumption that there are no heat losses on the free surface or equivalently that the heat transfer coefficient of the liquid-air interface is small: it is realistic to expect the air to be a poor heat conductor so that the interface is perfectly insulated from the air. Finally, Eq. (2d) is the kinematic boundary condition.

With the exception of surface tension, the liquid film properties, are assumed to be constant and independent of temperature. This is equivalent to a Boussinesq approximation (see, e.g., Leal[33]), which is applicable, provided that the temperature variations in the fluid are not large, and hence the wall temperature should not increase rapidly in the streamwise direction. With regards to density variations with temperature in particular, one could also define a Grashof or a Rayleigh number proportional to the thermal expansion coefficient of the liquid and the characteristic temperature scale γh_0. For thin films and since the thermal expansion coefficient is typically small for usual liquids, the Grashof number would be small, provided that γ is not large, so that buoyancy can be safely neglected.

Equations (1)–(4) have the Nusselt solution corresponding to the plane-parallel base state,

$$\frac{\partial^2 U}{\partial y^2} = -\frac{g\sin\theta}{\nu}, \tag{5a}$$

$$\frac{\partial P}{\partial y} = -\rho g\cos\theta, \tag{5b}$$

$$U\frac{\partial \Theta}{\partial x} = a\frac{\partial^2 \Theta}{\partial y^2}, \tag{5c}$$

with a constant thickness,

$$h = h_0. \tag{5d}$$

Equations (5a)–(5c) are subject to the interfacial boundary conditions at $y=h_0$,

$$\kappa\frac{\partial T}{\partial x} + \mu\frac{\partial U}{\partial y} = 0, \quad \frac{\partial T}{\partial y} = 0, \tag{5e}$$

and the wall boundary conditions at $y=0$,

$$U = 0, \quad T = \gamma x. \tag{5f}$$

The solution of the system in (5a)–(5f) has a velocity profile $U(y)$ given by a second-order polynomial,

$$U = \frac{gh_0^2}{\nu}\sin\theta\left(\eta - \frac{1}{2}\eta^2\right) - \frac{\kappa\gamma h_0}{\mu}\eta, \quad \eta = \frac{y}{h_0}, \tag{6a}$$

and a temperature profile given by a fourth-order polynomial,

$$\Theta = \gamma x + \frac{\gamma h_0^3}{\mu a}\left[\left(\frac{1}{2}\kappa\gamma - \frac{1}{3}\rho g\sin\theta\right)\eta + \frac{1}{6}(\rho g h_0\sin\theta - \kappa\gamma)\eta^3 - \frac{1}{24}\rho g h_0\sin\theta\eta^4\right]. \tag{6b}$$

Clearly the velocity and temperature fields are coupled already in the plane-parallel flow through the constant temperature gradient γ. For a uniform temperature distribution along the wall, i.e., $\gamma=0$ so that $\Theta=0$, there is no coupling between the velocity and temperature fields. This is to be expected, since for $\gamma=0$ and a zero heat flux on the free surface, the temperature is everywhere uniform and equal to the wall temperature.

We now utilize the Nusselt flat film solution to introduce the following nondimensionalization:

$$(x,y,z) \to (x,y,z)h_0, \quad h \to hh_0, \quad \mathbf{v} \to \mathbf{v}u_0,$$

$$t \to \frac{h_0}{u_0}t, \quad p \to \rho u_0^2 p, \quad T \to \gamma h_0 T,$$

where $u_0=gh_0^2\sin\theta/(3\nu)$ is the average velocity of the plane-parallel flow in the absence of thermocapillary forces. This nondimensionalization leads to the following dimensionless groups:

$$\mathrm{Re} = \frac{u_0 h_0}{\nu} = \frac{1}{3}\frac{gh_0^3}{\nu^2}\sin\theta, \quad \text{Reynolds number;}$$

$$\mathrm{We} = \frac{\sigma_0}{\rho h_0 u_0^2} = \frac{3^2\sigma\nu^2}{\rho g^2 h_0^5\sin^2\theta}, \quad \text{Weber number;}$$

$$\mathrm{Bo} = \frac{\rho g h_0}{\kappa\gamma}\sin\theta, \quad \text{dynamic Bond number;}$$

$$\mathrm{Pr} = \frac{\nu}{a}, \quad \text{Prandtl number;}$$

$$\mathrm{Pe} = \mathrm{Re}\,\mathrm{Pr} = \frac{u_0 h_0}{a}, \quad \text{Péclet number.}$$

The thermocapillary effect is described by the dynamic Bond number, which is the ratio between gravitational and Marangoni forces and is effectively an inverse modified Marangoni number. Note that $\mathrm{Bo}\to\infty$ corresponds to the case of strong gravitation compared to the Marangoni forces or to the problem of a falling film in the absence of Marangoni effects: this can occur when $\kappa=0$, in which case obviously we have no Marangoni effects, or $\gamma=0$, in which case and as we have already emphasized, the temperature is everywhere uniform and equal to the wall temperature. It is important to point out that $\gamma=0$ corresponds to the problem of a film falling down a uniformly heated wall analyzed by Goussis and Kelly,[15] Kalliadasis *et al.*,[19] Trevelyan and Kalliadasis,[24] Ruyer-Quil *et al.*,[25] and Scheid *et al.*[26] However, these authors assumed heat losses on the free surface instead of an isolated free surface assumed here. Hence, we cannot obtain from our problem statement the thermocapillary instability results in Refs. 15, 19, and 24–26 as a particular case.

Our system is governed by four dimensionless groups and the inclination angle, a total of five parameters: Re, We, Bo, Pr, and θ. Let us now introduce the Kapitza number[16]

$$\Gamma=\frac{\sigma_0}{\rho}\nu^{-4/3}g^{-1/3}, \tag{7a}$$

which depends on the liquid properties only and not the flow conditions. Since

$$\mathrm{We}=\frac{3^{1/3}\Gamma}{\mathrm{Re}^{5/3}(\sin\theta)^{1/3}}, \tag{7b}$$

the relevant groups are Re, Γ, Bo, Pr, and θ. Hence, for given liquids, the number of pertinent parameters can be further reduced to three: Re, Bo, and θ. Therefore for a fixed inclination angle and given liquids we have only two relevant parameters, Re and Bo, e.g., the vertical-plane case for fixed liquids is a two-parameter problem only.

Using the above nondimensionalization, the velocity and temperature distributions in (6a) and (6b) are written as

$$U=3\left(y-\frac{1}{2}y^2\right)-\frac{3}{\mathrm{Bo}}y, \tag{8a}$$

$$\Theta=x+\mathrm{Pe}\left[\left(\frac{3}{2\mathrm{Bo}}-1\right)y+\frac{1}{2}\left(1-\frac{1}{\mathrm{Bo}}\right)y^3-\frac{1}{8}y^4\right], \tag{8b}$$

where $\eta\equiv y$ due to the normalization with h_0. We can now obtain from Eq. (8a) the flow rate Q in the x direction,

$$Q=\int_0^1 U\,dy=1-\frac{3}{2\,\mathrm{Bo}}.$$

The value $\mathrm{Bo}=3/2$, which gives $Q=0$, marks the onset of a return flow in the system: $\mathrm{Bo}\gtrless 3/2$ leads to $Q\gtrless 0$. With $\mathrm{Bo}\to\infty$, gravitation is strong compared to the Marangoni forces, or the latter are absent and all the flow is directed downstream with $U\sim 3[y-(1/2)y^2]$. On the other hand, with $\mathrm{Bo}\to 0$, gravitation is weak compared to the Marangoni forces and all the flow is directed upstream with a linear velocity profile, $U\sim-(3/\mathrm{Bo})y$.

Orr-Sommerfeld and linearized energy equations

We now consider the stability of the Nusselt flat film solution to infinitesimal disturbances of the form

$$u=U+\varepsilon\hat{u}E,\quad v=\varepsilon\hat{v}E,\quad w=\varepsilon\hat{w}E,$$
$$T=\Theta+\varepsilon\hat{\theta}E,\quad h=1+\varepsilon\hat{h}E,\quad E=\mathrm{e}^{i(\mathbf{k}\cdot\mathbf{x}-\alpha ct)}, \tag{9}$$

where $\mathbf{x}=[x\ z]^t$, $\mathbf{k}=[\alpha\ \beta]^t$ is the wavenumber vector in the (x,z) plane, and c is the complex velocity of the infinitesimal perturbations. By substituting these expressions into the dimensionless version of the system in (1)–(4), utilizing (8), and taking the limit $\varepsilon\to 0$, we obtain the following linearized boundary-value problem:

$$i\alpha(U-c)\hat{u}+U'\hat{v}=-i\alpha\hat{p}+\frac{1}{\mathrm{Re}}[\hat{u}''-(\alpha^2+\beta^2)\hat{u}], \tag{10a}$$

$$i\alpha(U-c)\hat{v}=-\hat{p}'+\frac{1}{\mathrm{Re}}[\hat{v}''-(\alpha^2+\beta^2)\hat{v}], \tag{10b}$$

$$i\alpha(U-c)\hat{w}=-i\beta\hat{p}+\frac{1}{\mathrm{Re}}[\hat{w}''-(\alpha^2+\beta^2)\hat{w}], \tag{10c}$$

$$i\alpha(U-c)\hat{\theta}+\Theta'\hat{v}+\hat{u}=\frac{1}{\mathrm{Pe}}[\hat{\theta}''-(\alpha^2+\beta^2)\hat{\theta}], \tag{10d}$$

$$\hat{v}'+i(\alpha\hat{u}+\beta\hat{w})=0, \tag{10e}$$

$y=1$:

$$\hat{p}-\frac{3}{\mathrm{Re}}\cot\theta\hat{h}-(\alpha^2+\beta^2)\mathrm{We}\hat{h}-\frac{2}{\mathrm{Re}}(\hat{v}'-i\alpha U'\hat{h})=0, \tag{11a}$$

$$\frac{3}{\mathrm{Bo}}i\alpha\hat{\theta}+\hat{u}'+i\alpha\hat{v}+U''\hat{h}=0, \tag{11b}$$

$$\frac{3}{\mathrm{Bo}}i\beta\hat{\theta}+\hat{w}'+i\beta\hat{v}=0, \tag{11c}$$

$$\hat{v}=i\alpha(U-c)\hat{h}, \tag{11d}$$

$$\hat{\theta}'+\Theta''\hat{h}-i\alpha\hat{h}=0, \tag{11e}$$

$y=0$:

$$\hat{u}=\hat{v}=\hat{w}=\hat{\theta}=0, \tag{12}$$

where primes denote differentiation with respect to y.

The system in (10)–(12) is the Orr-Sommerfeld and linearized energy equations for the problem of a film falling down an inclined plane heated with a downward linearly increasing temperature distribution. These are the basic equations for the analysis to follow. We note that due to the coupling between the fluid flow and heat transport, Squire's theorem does not apply in our system. Hence, three-dimensional perturbations described by Eqs. (10)–(12) can-

not be transformed to equivalent two-dimensional ones by a suitable rotation of the coordinate system (also see the comment by Smith and Davis[9] in their study of the Marangoni instability of a horizontal liquid layer).

We also note that heat losses on the interface would amplify the Marangoni effect. As was already pointed out, for a uniformly heated wall there is no Marangoni effect in the absence of heat losses. Heat losses induce a Marangoni instability, which is amplified by increasing the heat losses; see, e.g., Kalliadasis *et al.*,[19] Trevelyan and Kalliadasis[24] and Scheid *et al.*[26] The key to this amplification is the fact that increasing the dimensionless heat transfer coefficient leads to larger free-surface temperature gradients in the x direction, which in turn enhance the Marangoni effect. In the problem considered here, we have a free-surface temperature gradient in the x direction to begin with: it is imposed by the downward linearly increasing temperature distribution on the wall. As a consequence, we have a Marangoni effect in the absence of heat losses. Hence, heat losses would just amplify this Marangoni effect. Of course this statement can only be verified with an analysis of the full system. However, we note that heat losses on the interface would alter the velocity of the base flow from $U=U(y)$ to $U=U(x,y)$, which would significantly complicate the Orr-Sommerfeld problem. Moreover, in this case asymptotic analysis of the Orr-Sommerfeld problem would not be possible.

We close this section with a comment on the limits of small Reynolds and Péclet numbers. The linearized equations in (10)–(12) describe the competition between two effects: inertia—for surface transverse waves this is the usual Kapitza hydrodynamic mode of instability for a falling film—and the Marangoni mode due to the thermocapillary stresses induced by the downward increasing wall temperature gradient—as we shall demonstrate this instability leads to long-wave surface transverse waves and short-wave rolls. This competition is monitored by the Reynolds number in (10a)–(10c) and by the Péclet number in (10d).

For $\mathrm{Pe}\to 0$ (because $\mathrm{Pr}\to 0$ like in liquid metals), the temperature field is slaved to the velocity field and one can drop the left-hand side of (10d). This then "freezes" the Marangoni mode, the time evolution is the one for the velocity field, and the system is simply driven by inertia or in the particular case of surface transverse instabilities by the Kapitza mode appropriately modified by the Marangoni effect. On the other hand, for $\mathrm{Re}\to 0$ (while Pe remains finite), the velocity field is slaved to the temperature field and one can drop the left-hand-side and pressure terms in (10a)–(10c). This then "freezes" inertia (or the Kapitza mode for surface transverse instabilities), the time evolution is the one for the temperature field and the system is simply driven by the Marangoni forces.

III. TRANSVERSE INSTABILITY AND SURFACE WAVES

Let us consider surface waves and obtain the evolution of two dimensional disturbances, $\partial/\partial z=0$ and $\hat{w}=0$. We define the complex streamfunction

$$\hat{u}=\phi', \tag{13a}$$

$$\hat{v}=-i\alpha\phi, \tag{13b}$$

so that the continuity equation in (10e) is trivially satisfied and the boundary-value problem in (10)–(12) is now written as

$$\phi''''-2\alpha^2\phi''+\alpha^4\phi=i\alpha\,\mathrm{Re}[(U-c)(\phi''-\alpha^2\phi)-U''\phi], \tag{14a}$$

$$\hat{\theta}''-\alpha^2\hat{\theta}=i\alpha\mathrm{Pe}\left((U-c)\hat{\theta}-\Theta'\phi+\frac{\phi'}{i\alpha}\right), \tag{14b}$$

$y=1$:

$$\phi'''-3\alpha^2\phi'+i\alpha\,\mathrm{Re}(c-U)\phi'-3i\alpha\cot\theta\hat{h} - i\alpha^3\,\mathrm{Re}\,\mathrm{We}\,\hat{h}-i\alpha\mathrm{Re}U'\phi-2\alpha^2U'\hat{h}=0, \tag{15a}$$

$$\phi''+\alpha^2\phi-3\hat{h}+i\alpha r\hat{\theta}=0, \tag{15b}$$

$$\phi=\left(c-\frac{3}{2}+r\right)\hat{h}, \tag{15c}$$

$$\hat{\theta}'=i\alpha\hat{h}-\Theta''\hat{h}, \tag{15d}$$

$y=0$: $$\phi=\phi'=\hat{\theta}=0, \tag{16}$$

where $r=3/\mathrm{Bo}$, which is effectively a Marangoni number.

We now consider long-wave perturbations, $\alpha\to 0$. Accordingly, we seek our solution in the form (it turns out that even terms of this expansion are real and odd purely imaginary),

$$\phi\sim\phi_0+i\alpha\phi_1+\alpha^2\phi_2+i\alpha^3\phi_3,$$

$$\hat{\theta}\sim\hat{\theta}_0+i\alpha\hat{\theta}_1+\alpha^2\hat{\theta}_2+i\alpha^3\hat{\theta}_3, \tag{17}$$

$$c\sim c_0+i\alpha c_1+\alpha^2c_2+i\alpha^3c_3.$$

Substituting these expansions into (14)–(16) allows for a sequential solution of the eigenvalue problem by separating powers of α. Note that (15c) is solved for $\hat{h}$, which is then substituted into (15a), (15b), and (15d), which together with (16) are the six boundary conditions required for the solution of (14a) and (14b). To illustrate the solution procedure, let us consider the $O(1)$ problem

$$\phi_0''''=0, \tag{18a}$$

$$\hat{\theta}_0''=\mathrm{Pe}\,\phi_0', \tag{18b}$$

subject to the boundary conditions

$y=1$:

$$\phi_0'''=0, \tag{19a}$$

$$\phi_0'' - \frac{3\phi_0}{c_0 - \frac{3}{2} + r} = 0, \tag{19b}$$

$$\hat{\theta}_0' = -\mathrm{Pe}\left(\frac{3}{2} - r\right)\frac{\phi_0}{c_0 - \frac{3}{2} + r}, \tag{19c}$$

$$y = 0: \quad \phi_0 = \phi_0' = \hat{\theta}_0 = 0. \tag{20}$$

The solution to (18a) which satisfies (19a) and (20) is $\phi_0 = Ay^2$, which when substituted in (19b) yields $A(c_0 - 3 + r) = 0$. For a nontrivial ϕ_0, $A \neq 0$ so that $c_0 = 3 - r$ while ϕ_0 is known within an arbitrary constant. Hence, the eigenvalue is determined from the tangential stress balance, where the Marangoni effect is predominant. Once ϕ_0 is known, the solution for $\hat{\theta}_0$ that satisfies (19c) and (20) can be easily found to be $\hat{\theta}_0 = (2/3)\mathrm{Pe}\, A[(1/2)y^3 - (3-r)y]$, so that ϕ_0 and $\hat{\theta}_0$ are polynomials in y. In fact, at all orders ϕ and $\hat{\theta}$ are found to be polynomials in y.

Here we summarize the solution for a vertical plane:

$$c_0 = 3 - r, \tag{21a}$$

$$c_1 = \mathrm{Re}\left[\frac{1}{2} r\,\mathrm{Pr}\left(\frac{5}{2} - r\right) + \frac{2}{5}(3 - r)\right], \tag{21b}$$

$$c_2 = \mathrm{Re}^2\left(a_1 r^3 + a_2 r^2 + a_3 r - \frac{12}{6}\right) + \frac{7}{6}\left(r - \frac{18}{7}\right), \tag{21c}$$

$$c_3 = -\frac{\mathrm{We\,Re}}{3} + \mathrm{Re}^3\left(a_4 r^4 + a_5 r^3 - a_6 r^2 - a_7 r - \frac{75872}{25025}\right) - \mathrm{Re}\left(a_8 r^2 - a_9 r - \frac{1413}{224}\right), \tag{21d}$$

where

$$a_1 = \frac{1}{8}\mathrm{Pr}^2 - \frac{2}{15}\mathrm{Pr}, \quad a_2 = \frac{1}{160}\mathrm{Pr}^2 + \frac{563}{480}\mathrm{Pr} - \frac{11}{96},$$

$$a_3 = -\frac{4}{5}\mathrm{Pr}^2 - \frac{173}{80}\mathrm{Pr} + \frac{205}{224},$$

$$a_4 = -\frac{131}{2016}\mathrm{Pr}^3 - \frac{259}{1440}\mathrm{Pr}^2 + \frac{11}{288}\mathrm{Pr},$$

$$a_5 = \frac{33673}{60480}\mathrm{Pr}^3 + \frac{297131}{302400}\mathrm{Pr}^2 - \frac{977}{1350}\mathrm{Pr} + \frac{137}{4158},$$

$$a_6 = \frac{620069}{806400}Pr^3 + \frac{25591}{44800}\mathrm{Pr}^2 - \frac{2805359}{806400}\mathrm{Pr} + \frac{544441}{1108800},$$

$$a_7 = \frac{73393}{134400}\mathrm{Pr}^3 + \frac{26699}{13440}\mathrm{Pr}^2 + \frac{8717}{1792}\mathrm{Pr} - \frac{10508741}{4804808},$$

$$a_8 = \frac{3}{2}\mathrm{Pr} - \frac{19}{180}, \quad a_9 = \frac{291}{86}\mathrm{Pr} + \frac{5417}{1680}\mathrm{Pr}.$$

Notice that at $r = 0$, which implies $\mathrm{Bo} \to \infty$, our solution coincides with that for the free-falling film flow.[35,36]

For an arbitrary inclination angle, the solution is too lengthy and is not needed here. However, for the case of strong capillary forces, $\mathrm{We} \gg 1$ or equivalently $\Gamma \gg 1$ (for water at 25°, $\Gamma = 2850$) and for an arbitrary angle, $c_3 \sim \mathrm{We\,Re}/3$—We Re/3 is much larger than the rest of the terms in c_3 for an arbitrary angle—so that the solution for the real and imaginary parts of the eigenvalue can be simplified to

$$c_r \sim (3 - r) + \alpha^2 c_2, \tag{22a}$$

$$c_i \sim \alpha\left[\frac{2}{5}\mathrm{Re}(3 - r) + \frac{1}{2} r\,\mathrm{Pe}\left(\frac{5}{2} - r\right) - \cot\theta - \frac{\alpha^2\,\mathrm{We\,Re}}{3}\right], \tag{22b}$$

where c_2 is given by Eq. (21c). From (22a) it follows that with an accuracy of $O(\alpha^2)$, the infinitesimal wave velocity is $3 - r$, which decreases with increasing thermocapillary forces. Interestingly, c_r changes sign at $r = 3$. Note also that (22b) shows the competition between the two instabilities: the Kapitza instability controlled by the Reynolds number and the Marangoni instability controlled by the Péclet/Reynolds number for heat transport. These two modes contribute the terms $(2/5)\mathrm{Re}(3 - r)$ and $(1/2)\mathrm{Pe}[(5/2) - r]$ in the growth rate of the infinitesimal disturbances. The Kapitza mode is appropriately modified by the Marangoni effect, which is responsible for the $-(2/5)r$ term. Indeed, the usual parabolic profile for a free-falling film is modified by the Marangoni effect, which contributes the linear term $-ry$ to the velocity field in (8a), which in turn originates from the interfacial boundary condition in (5e).

The neutral curve, $\alpha c_i = 0$, can be readily obtained from (22b). This gives two branches of the neutral curve, $\alpha_0 = 0$ (with α_0 being the neutral wavenumber) and

$$\alpha_0^2 = \frac{3}{\mathrm{We}}\left[\frac{2}{5}(3 - r) + \frac{1}{2} r\,\mathrm{Pr}\left(\frac{5}{2} - r\right) - \frac{\cot\theta}{\mathrm{Re}}\right], \tag{23}$$

so that the base state is unstable to perturbations with wavenumbers $\alpha < \alpha_0$. From (22b) we can also obtain the critical condition for the onset of the instability by simply setting the $O(\alpha)$ term of c_i equal to zero:

$$\left(\frac{\cot\theta}{\mathrm{Re}}\right)_* = \frac{6}{5} + r\left(\frac{5}{4}\mathrm{Pr} - \frac{2}{5} - \frac{r}{2}\mathrm{Pr}\right). \tag{24}$$

This expression is reduced for $r = 0$ to the well-known critical condition for a free-falling film:[35,36]

$$\left(\frac{\cot\theta}{\mathrm{Re}}\right)_* = \frac{6}{5}. \tag{25}$$

Beyond onset, the isothermal film undergoes a sequence of wave transitions that eventually lead to a train of solitary

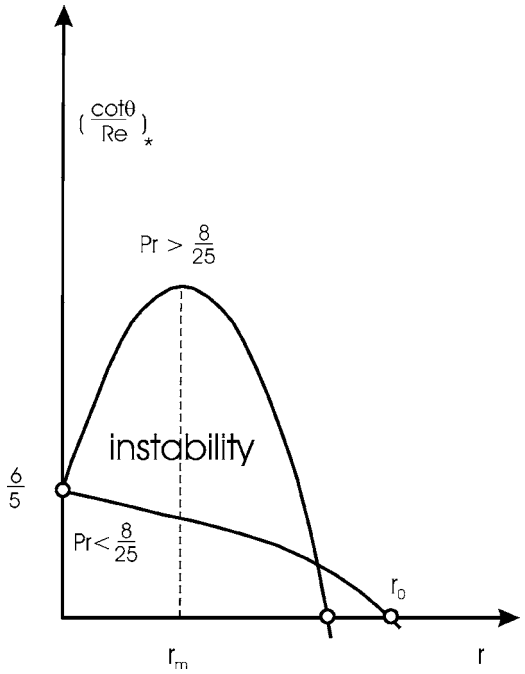

FIG. 2. Critical curve as a function of r for different Pr. The onset of instability for the free-falling film occurs at $r=0$ and $(\cot\theta/\mathrm{Re})_*=6/5$. For instability, $r<r_0$ and $\cot\theta/\mathrm{Re}<(\cot\theta/\mathrm{Re})_*$ (below the critical curve). For $\mathrm{Pr}>8/25$, upon increasing the temperature gradient the flow is first destabilized while by further increasing the temperature gradient the flow becomes more stable. For $\mathrm{Pr}<8/25$, increasing the Marangoni forces stabilizes the flow. For $r>r_0$ the flow is always stable.

pulses. This stage of the instability has been scrutinized by Chang[37] and Chang and Demekhin.[38]

In contrast to the case of a film falling down a uniformly heated wall, where the Marangoni effect reduces the critical Reynolds number and hence has a destabilizing influence,[15,19,24–27] in our case it can either stabilize or destabilize the flow. Figure 2 depicts the critical condition in (24). The slope at $r=0$ is given by $d(\cot\theta/\mathrm{Re})_*/dr=(5/4)\mathrm{Pr}-(2/5)$, which is $\gtrless 0$ for $\mathrm{Pr}\gtrless 8/25$. For $\mathrm{Pr}>8/25$, increasing r, i.e., increasing the wall temperature gradient and hence the thermocapillary forces, first causes $(\cot\theta/\mathrm{Re})_*$ to increase (and hence it has a destabilizing influence as the critical Reynolds number decreases) up to the maximum of the critical curve with coordinates

$$r_m=\frac{5\left(\mathrm{Pr}-\frac{8}{25}\right)}{4\,\mathrm{Pr}}, \tag{26a}$$

$$\left(\frac{\cot\theta}{\mathrm{Re}}\right)_m=\frac{6}{5}+\frac{25}{32}\left(\frac{\left(\mathrm{Pr}-\frac{8}{25}\right)^2}{\mathrm{Pr}}\right). \tag{26b}$$

For water at 25° with $\mathrm{Pr}=7$ this gives $(\cot\theta/\mathrm{Re})_m=6.2$, more than five times larger than the critical value 6/5 corresponding to the standard falling film flow with no Marangoni effect.

However, further increasing the temperature gradient and for $r>r_m$, $(\cot\theta/\mathrm{Re})_*$ decreases as r increases, which has a stabilizing effect as the critical Reynolds number in this region increases. On the other hand, for $\mathrm{Pr}<8/25$, $(\cot\theta/\mathrm{Re})_*$ monotonically decreases as r increases and in this case the thermocapillary forces have a stabilizing influence. Eventually at $r=r_0$ defined from

$$r_0=\frac{5}{4}-\frac{2}{5\,\mathrm{Pr}}+\sqrt{\frac{25}{16}+\frac{7}{5\,\mathrm{Pr}}+\frac{4}{25\,\mathrm{Pr}^2}}, \tag{27}$$

the thermocapillary forces completely suppress the instability as at this point $(\cot\theta/\mathrm{Re})_*=0$ (hence an infinite critical Reynolds number), as illustrated in Fig. 2.

The term $(6/5)-(2/5)r$ is the Kapitza contribution to the critical Reynolds number. The role of the Marangoni effect here is simply to dampen the usual hydrodynamic mode of instability of a free-falling film through the term $-(2/5)r$. The term $r\,\mathrm{Pr}[(5/4)-(r/2)]$, on the other hand, is due to the Marangoni instability and depends on both the Péclet number and r. Note that Pr appears in a product with r so that if $r\to 0$ (gravitation is strong compared to the Marangoni forces or simply there is no Marangoni effect), there is no influence of the Péclet number on the instability threshold. Similarly, if $\mathrm{Pe}\to 0$, freezes the Marangoni effect and the system is driven by the Kapitza instability, appropriately modified by the Marangoni forces. On the other hand, $\mathrm{Re}\to 0$ freezes the Kapitza instability (also see our discussion in the previous section), and the system is driven by the Marangoni forces that contribute a term $(1/2)r\,\mathrm{Pe}[(5/2)-r]$ in the growth rate. This term destabilizes the system for $r<5/2$.

As a result, different liquids will exhibit a different behavior with respect to the instabilities considered here, depending on their Prandtl number. For falling films with liquids having small Prandtl numbers, e.g., liquid metals, the waves on the films are controlled by the Kapitza mode. For falling films with liquids having large Prandtl numbers, e.g., silicone oils, the waves are controlled by the Marangoni instability. This competition between the two Reynolds numbers occurs throughout this study.

Note that the criticality condition obtained by Miladinova *et al.*[31,32] using a long-wave (lubrication) approximation (their condition expresses the critical Reynolds number, Re_* as a function of $r\mathrm{Re}_*$) is in agreement with our condition in (24) obtained from a long-wave expansion of the full Orr-Sommerfeld/linearized energy equations. This is not surprising, as the lubrication approximation being a regular perturbation expansion of the full Navier-Stokes and energy equation should be exact close to criticality. In fact, the lubrication approximation is only valid close to criticality and breaks down further from criticality. Similarly, the long-wave expansion of the Orr-Sommerfeld eigenvalue problem performed here breaks down away from criticality. We shall return to this point in Sec. V, where we construct the numerical solution of the Orr-Sommerfeld eigenvalue problem. Also note that the studies by Miladinova *et al.* focused on liquids with $\mathrm{Pr}\gtrsim 1$ and hence did not uncover the critical value $\mathrm{Pr}=8/25$ below which the critical Reynolds number increases monotonically with r and the thermocapillary forces have a stabilizing effect. In addition, if the critical curves $(r\,\mathrm{Re}_*,\mathrm{Re}_*)$ for $\theta=\pi/4$ of Miladinova *et al.* are extended for

larger $r\,\mathrm{Re}_*$ than those considered by these authors, it becomes evident that a minimum for Re_* exists for all $\mathrm{Pr} \geqslant 8/25$ (for $\mathrm{Pr}=1$, $\theta=\pi/4$ this occurs at $r\,\mathrm{Re}_* \sim 0.5$) so that thermocapillary stresses initially destabilize and then stabilize the system, in agreement with Fig. 2.

Finally, note that the neutral value r_0 depends on Pr only and in contrast to r_m this dependence is weak. Indeed, when we consider the whole range of Prandtl numbers, $0 \leqslant \mathrm{Pr} < \infty$, the neutral value of r remains within the range $2.5 < r_0 < 3$: $\mathrm{Pr} \to \infty$ gives $r_0=2.5$, and for $\mathrm{Pr}=0$, $r_0=3$. For water at 25°, $r_0=2.52$. As a consequence, with $r<r_0<3$, to leading order in α, $c_r \sim 3-r>0$. This implies that the instability always assumes the form of surface waves traveling downstream (with velocity $3-r$). Therefore, even though for $\mathrm{Bo}<3/2$, or equivalently $r<2$, part of the base flow moves upstream (see Sec. II), the disturbances travel downstream, but with a velocity <3, which is the velocity of the infinitesimal disturbances for the usual Kapitza hydrodynamic mode of the instability. We also note that the average velocity of the mean flow given in (8a) $\langle U\rangle = 1-(r/2)$ so that $c_r \sim 3-r>\langle U\rangle$ for $r<4$. Since for the instability to be seen, $r<r_0(<3)$, we always have $c_r>\langle U\rangle$ and the disturbances always travel faster than the mean flow, even though the Marangoni effect reduces their speed. Evidently, for $r>3$ the disturbances do travel upstream, but they are stable, as in this case we are above the critical curve in Fig. 2.

IV. LONGITUDINAL AND TRANSVERSE ROLLS

For a horizontal layer heated uniformly from below, the Marangoni effect is also responsible for another kind of monotonic instability. As was shown by Pearson[4] and Smith,[7] this instability leads to convective cells (sometimes referred to as "rolls"). Note that there is no preferred direction in the orientation of the cells. As we discussed in the Introduction, for this kind of instability deformation of the interface does not play an important role provided that certain conditions are satisfied, e.g., small temperature gradients across the film and small film thicknesses—for a detailed discussion of this point see Velarde *et al.*[6] and Rednikov *et al.*[39]

Then, if for a horizontal layer there is no preferred direction in the orientation of the convective cells, for an inclined plane heated uniformly from below, the preferred direction for thermocapillary convection should be the longitudinal direction, $\alpha=0$, as shown by Goussis and Kelly.[15] In this case there is no influence of the mean flow and the instability has a purely thermal origin.

To analyze this instability in our case, we set $\hat{h}=0$ in (10)–(12), hence assuming that the free surface is nondeformable. For perturbations along the longitudinal coordinate only, $\alpha=0$ and $\beta\neq 0$. We then have

$$\lambda\hat{u} + U'\hat{v} = \frac{1}{\mathrm{Re}}(\hat{u}'' - \beta^2\hat{u}), \tag{28a}$$

$$\lambda\hat{v} = -\hat{p}' + \frac{1}{\mathrm{Re}}(\hat{v}'' - \beta^2\hat{v}), \tag{28b}$$

$$\lambda\hat{w} = -i\beta\hat{p} + \frac{1}{\mathrm{Re}}(\hat{w}'' - \beta^2\hat{w}), \tag{28c}$$

$$\lambda\hat{\theta} + \Theta'\hat{v} + \hat{u} = \frac{1}{\mathrm{Pe}}(\hat{\theta}'' - \beta^2\hat{\theta}), \tag{28d}$$

$$\hat{v}' + i\beta\hat{w} = 0, \tag{28e}$$

subject to the boundary conditions

$y=1$:

$$\hat{v} = 0, \tag{29a}$$

$$\hat{u}' = 0, \tag{29b}$$

$$r\beta^2\hat{\theta} + \hat{v}'' = 0, \tag{29c}$$

$$\hat{\theta}' = 0, \tag{29d}$$

and

$$y=0: \quad \hat{u} = \hat{v} = \hat{w} = \hat{\theta} = 0, \tag{30}$$

where $\lambda = -i\alpha c$ is the growth rate. Equations (28a)–(28d) express the competition between the two Reynolds numbers: (28a)–(28c) are controlled by the Reynolds number and (28d) is controlled by the Péclet number. For $\mathrm{Re}\to 0$ inertia is not important and the system is completely driven by the Marangoni forces. On the other hand, for $\mathrm{Pe}\to 0$ the Marangoni forces are negligible and the system is dominated by inertia.

The solution of (28)–(30) can be constructed analytically as a combination of hyperbolic sines and cosines and polynomials in y. The procedure is sketched in the Appendix. The solution has a cumbersome form and is not needed here. Instead we shall only consider the neutral case, $\lambda=0$. Equations (28)–(30) then reduce to

$$\hat{v}^{IV} - 2\beta_0^2\hat{v}'' + \beta_0^4\hat{v} = 0, \tag{31a}$$

$$\hat{u}'' - \beta_0^2\hat{u} = \mathrm{Re}\,U'\hat{v}, \tag{31b}$$

$$\hat{\theta}'' - \beta_0^2\hat{\theta} = \mathrm{Pe}(\Theta'\hat{v} + \hat{u}), \tag{31c}$$

subject to the boundary conditions

$y=1$:

$$\hat{v} = 0, \tag{32a}$$

$$\hat{u}' = 0, \tag{32b}$$

$$r\beta_0^2\hat{\theta} + \hat{v}'' = 0, \tag{32c}$$

$$\hat{\theta}' = 0, \tag{32d}$$

and

$$y=0: \quad \hat{u}=\hat{v}=\hat{v}'=\hat{\theta}=0, \tag{33}$$

where β_0 is the neutral wavenumber. Hence $\hat{w}$ has been eliminated from the problem and can be readily evaluated from (28e) once $\hat{v}$ is known, while one of (29b) and (29c) can be used to obtain $\hat{p}$.

Note that in contrast to the case of a wall with a constant temperature, where the mean flow is not present in the eigenvalue problem for longitudinal rolls (see Goussis and Kelly[15]), in our case, there is coupling between velocity perturbations and the mean flow due to the temperature gradient along the wall: note the presence of U' in (31b) and r in (32c). Hence, we can expect a significant influence of the parameter r on the stability results.

The solution of (31)–(33) can be constructed analytically. The problem can be significantly simplified by considering separately the case of large and small β_0, respectively, and by comparing the analytical results with a numerical solution of the full system in (31)–(33). The characteristic equation of (31a) is $(\delta^2-\beta_0^2)^2=0$ with roots $\delta_{1,2}=\delta_{3,4}=\pm\beta_0$ (two double roots). The solution then of (31a) that satisfies (32a) and (33) can be written as

$$\hat{v}=\sinh\beta_0 y-\beta_0 y\cosh\beta_0 y+(\beta_0\coth\beta_0 - 1)y\sinh\beta_0 y. \tag{34a}$$

Note that the solution is known within an arbitrary constant which without loss of generality has been set equal to unity. With $\beta_0\gg 1$, the above expression gives

$$\hat{v}=\mathrm{e}^{\beta_0 y}-y\mathrm{e}^{\beta_0 y}, \tag{34b}$$

where the $1/2$ factor resulting from the limit process has been absorbed within $\hat{v}$.

The solution to (31b) can then be readily obtained. It is a sum of the general solution of the corresponding homogeneous equation and a particular solution of the nonhomogeneous equation, which is obtained by using the method of variation of parameters. With $\beta_0\gg 1$, the solution to (31b) that satisfies (32b) and (33) can be written as

$$\hat{u}=\left(B+Cy+Dy^2+\frac{\mathrm{Re}}{2\beta_0}y^3\right)\mathrm{e}^{\beta_0 y}, \tag{35}$$

where

$$B=\frac{\mathrm{Re}\left(-\frac{1}{2}+\frac{1}{4}r\right)}{\beta_0}-\frac{\mathrm{Re}\left(\frac{3}{4}-\frac{1}{4}r\right)}{\beta_0^2}-\frac{\mathrm{Re}\left(\frac{3}{4}-\frac{1}{4}r\right)}{\beta_0^3}-\frac{3\,\mathrm{Re}}{4\beta_0^4},$$

$$C=\frac{\mathrm{Re}(3-r)}{2\beta_0}+\frac{\mathrm{Re}(6-r)}{4\beta_0^2}+\frac{3\,\mathrm{Re}}{4\beta_0^3},$$

$$D=-\frac{\mathrm{Re}(6-r)}{4\beta_0}-\frac{3\,\mathrm{Re}}{4\beta_0^2}.$$

The function $\Theta'\hat{v}+\hat{u}$ in (31c), required for the solution of $\hat{\theta}$, can then be written as

$$\hat{u}+\Theta'\hat{v}=(\bar{A}+\bar{B}y+\bar{C}y^2+\bar{D}y^3+\bar{E}y^4)\mathrm{e}^{\beta_0 y},$$

where

$$\bar{A}=\mathrm{Pe}\left(\frac{1}{2}r-1\right)+B, \quad \bar{B}=C-\mathrm{Pe}\left(\frac{1}{2}r-1\right),$$

$$\bar{C}=\mathrm{Pe}\left(\frac{3}{2}-\frac{1}{2}r\right)+D,$$

$$\bar{D}=-\frac{1}{2}\mathrm{Pe}-\mathrm{Pe}\left(\frac{3}{2}-\frac{1}{2}r\right)+\frac{\mathrm{Re}}{2\beta_0^2}, \quad \bar{E}=\frac{1}{2}\mathrm{Pe}.$$

With $\beta_0\gg 1$, the solution to (31c) that satisfies (33) can be written as

$$\frac{\hat{\theta}}{\mathrm{Pe}}=(M_0+M_1 y+M_2 y^2+M_3 y^3+M_4 y^4+M_5 y^5)\mathrm{e}^{\beta_0 y}, \tag{36a}$$

where

$$M_1=\frac{\bar{A}}{2\beta_0}-\frac{\bar{B}}{4\beta_0^2}+\frac{\bar{C}}{4\beta_0^3}-\frac{3\bar{D}}{8\beta_0^4}+\frac{3\bar{E}}{4\beta_0^5}, \tag{36b}$$

$$M_2=\frac{\bar{B}}{4\beta_0}-\frac{\bar{C}}{4\beta_0^2}+\frac{3\bar{D}}{8\beta_0^3}-\frac{3\bar{E}}{4\beta_0^4},$$

$$M_3=\frac{\bar{C}}{6\beta_0}-\frac{\bar{D}}{4\beta_0^2}+\frac{\bar{E}}{2\beta_0^3}, \quad M_4=\frac{\bar{D}}{8\beta_0}-\frac{\bar{E}}{4\beta_0^2}, \tag{36c}$$

$$M_5=\frac{\bar{E}}{10\beta_0}.$$

M_0 can then be easily obtained from the boundary condition in (32d):

$$M_0=-(M_1+M_2+M_3+M_4+M_5)-\frac{1}{\beta_0}(M_1+2M_2+3M_3+4M_4+5M_5). \tag{36d}$$

Substituting now (36a) into (32c) gives the dispersion relation. Equation (32c) originates from the tangential stress balance in (11) and the continuity equation in (28e). Hence, the eigenvalue for longitudinal rolls is effectively determined by the Marangoni forces, as was the case with the transverse and surface waves considered in the previous section.

The dispersion relation can be written as a series expansion in inverse powers of β_0:

$$\beta_0=\frac{1}{16\beta_0^2}\,\mathrm{Pe}^2\,r(3-2r)+\frac{1}{32\beta_0^3}\mathrm{Pe}(3\,\mathrm{Pe}-4\,\mathrm{Re})r^2+\frac{1}{32\beta_0^4}\mathrm{Pe}(15\,\mathrm{Re}-6\,\mathrm{Pe})r, \tag{37a}$$

and once again it is the competition between the two Reynolds numbers that determines the neutral curve. For β_0 now to be large, Pe must be taken as a large parameter, and for a

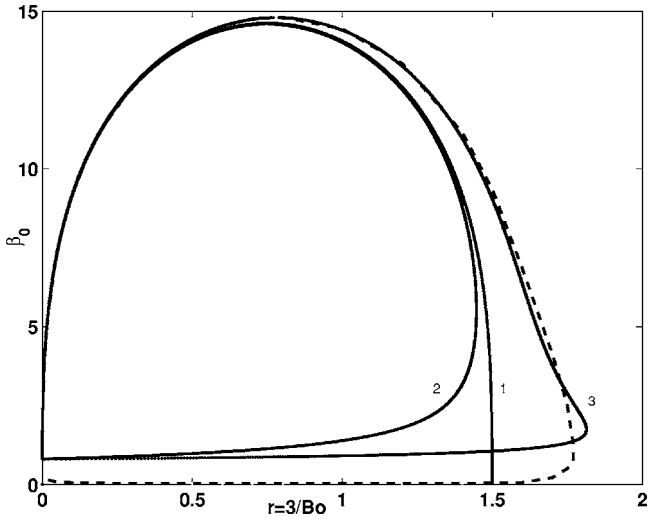

FIG. 3. Longitudinal instability for Pr=7 and Re=30. The instability occurs inside the region $r_1<r<r_2$; curve 1 corresponds to a one-term expansion given in (37b), curve 2 to two-term expansion from (37a), and curve 3 to all three terms in (37a). The dashed line is the numerical solution of the full system in (31)–(33). Short-wave rolls are predicted very well by (37a).

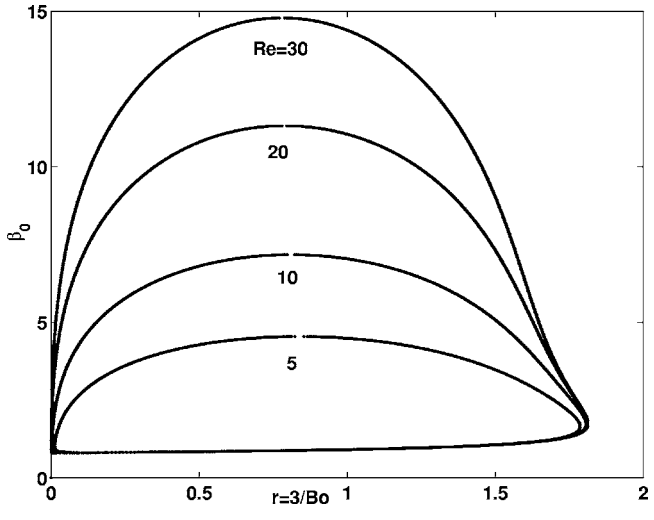

FIG. 4. Longitudinal instability obtained from (37a) for Pr=7 and different Reynolds numbers.

single term in the expansion, we simply have

$$\beta_0 \sim \left(\frac{\mathrm{Pe}^2\, r(3-2r)}{16}\right)^{1/3}, \tag{37b}$$

so that $\beta_0=O(\mathrm{Pe}^{2/3})$. Hence, short-wave longitudinal rolls are driven by the Marangoni effect only if the Reynolds number is sufficiently small, specifically $\mathrm{Re}\ll\mathrm{Pe}^{5/3}$, so that inertia terms in (37a) can be neglected.

Typical solutions with one, two, and all three terms, alongside a numerical solution of the full system in (31)–(33), are shown in Fig. 3 for Pr=7 and Re=30. The numerical scheme is based on a procedure similar to that described in the next section. We notice that even a one-term expansion captures the main features of the stability map, while the three-term expansion describes practically the whole instability region except for small β, where it overestimates the instability threshold with the numerically obtained threshold lying below the analytical prediction.

The instability consists of both long-wave and short-wave modes and occurs inside a finite region $r_1<r<r_2$ and, hence, there are two critical values of r. The existence of a small but finite $r_1(\neq 0)$ is difficult to see in the figure. Interestingly, for short convective rolls, r_2 is close to r_0 for long surface waves: for water at 25°, $r_0=2.52$, while $r_2=1.78$. Figure 4 depicts the instability region for different Reynolds numbers obtained from (37a). The region of instability grows as the Reynolds number increases, but the boundaries r_1 and r_2 remain practically unaltered.

The lower branch of unstable longitudinal rolls can be found by considering long waves. In the limit $\beta_0\to 0$, (34a) gives

$$\hat{v}=\left(1-\frac{1}{15}\beta_0^2\right)y^2-y^3+\frac{1}{6}\beta_0^2y^4-\frac{1}{10}\beta_0^2y^5+O(\beta_0^4), \tag{38}$$

where the factor $\beta_0^3/3$ multiplying the right-hand side of (34a) has been absorbed in $\hat{v}$. The solution now to (31b) that satisfies (32b) and (33) is

$$\begin{aligned}\hat{u}=&-\frac{1}{12}(r-3)y^4+\frac{1}{10}\left(\frac{r}{2}-3\right)y^5+\frac{1}{10}y^6+\left[\frac{1}{12}\left(\frac{r}{6}\right.\right.\\&\left.-\frac{1}{5}\right)y^3+\frac{1}{180}(r-3)y^4+\frac{1}{100}y^5-\frac{1}{120}\left(\frac{r}{6}-3\right)y^6\\&\left.+\frac{1}{280}\left(r-\frac{22}{3}\right)y^7+\frac{1}{140}y^8\right]\beta_0^2,\end{aligned} \tag{39}$$

where again terms of $O(\beta_0^4)$ and higher have been neglected.

For $\hat{\theta}$ only the $O(1)$ approximation is needed due to the presence of β_0^2 in (32c). This is simply given by

$$\begin{aligned}\hat{\theta}=&\left[\left(\frac{1}{28}-\frac{1}{30}r\right)\mathrm{Re}+\left(\frac{19}{420}-\frac{1}{40}r\right)\mathrm{Pe}\right]y+\left(\frac{1}{72}r\right.\\&\left.-\frac{1}{60}\right)\mathrm{Re}\,y^3+\left(\frac{1}{24}r-\frac{1}{12}\right)\mathrm{Pe}\,y^4-\left(\frac{1}{40}r-\frac{1}{20}\right)\mathrm{Pe}\,y^5\\&+\left[-\left(\frac{1}{360}r-\frac{1}{120}\right)\mathrm{Re}-\left(\frac{1}{60}r-\frac{1}{20}\right)\mathrm{Pe}\right]y^6\\&+\left[\left(\frac{1}{840}r-\frac{1}{140}\right)\mathrm{Re}+\left(\frac{1}{84}r-\frac{1}{21}\right)\mathrm{Pe}\right]y^7\\&+\left(\frac{1}{560}\,\mathrm{Re}+\frac{1}{112}\mathrm{Pe}\right)y^8.\end{aligned} \tag{40}$$

Substituting then (38) and (40) into (32c) yields the dispersion relation

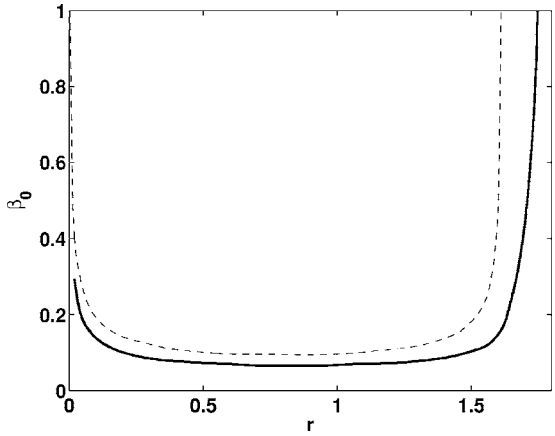

FIG. 5. Long-wave longitudinal instability for Pr=7 and Re=30. Dashed line: analytical solution in (41b). Solid line: numerical solution of the full system in (31)–(33).

$$4+\frac{2}{15}\beta_0^2 = r\,\mathrm{Pe}\,\beta_0^2\left[\left(\frac{13}{560}-\frac{11}{840}r\right)\mathrm{Pe}+\left(\frac{37}{1680}-\frac{53}{2520}r\right)\mathrm{Re}\right], \tag{41a}$$

and once more it is the competition between the two Reynolds numbers that determines the neutral curve. By taking now as a small parameter $1/Pe^2 \sim 1/(\mathrm{PeRe})$ and neglecting the term $(2/15)\beta_0^2$ in (41a), we obtain

$$\beta_0^2 \sim \frac{4}{r\,\mathrm{Pe}\left[\left(\frac{13}{560}-\frac{11}{840}r\right)\mathrm{Pe}+\left(\frac{37}{1680}-\frac{53}{2520}r\right)\mathrm{Re}\right]}. \tag{41b}$$

On the other hand, for $\mathrm{Pe}\gg\mathrm{Re}$, $\beta_0^2 \sim 4/[r\,\mathrm{Pe}^2(13/560)-(11/840)r]$, and in this case long-wave longitudinal rolls are driven by the Marangoni effect only. In Fig. 5 we compare the expression for long rolls in (41b) with the numerical solution of the full system in (31)–(33). The analytical solution is very close to the numerical one for all r.

Finally, note that longitudinal rolls for the problem considered here have also been examined by Ludviksson and Lightfoot.[30] These authors obtained numerically the neutral curves for longitudinal rolls from the full Orr-Sommerfeld eigenvalue problem but they used a different parametrization to the one adopted here: they represented the surface tension gradient κ as a function of the neutral wavenumber for different values of the flat film thickness h_0. Nevertheless, their results show that the unstable region is of a finite extent and grows with increasing h_0, in qualitative agreement with Fig. 4.

Consider now convective rolls that are oriented along the transverse direction, namely, $\alpha\neq 0$ and $\beta=0$. These rolls are not steady, but they propagate with a velocity close to the surface velocity $3/2-r$ for large α (recall that the velocity of transverse surface waves is close to $3-r$). In a frame moving with the surface velocity, the term $i\alpha(U-c)\hat{u}$ in Eq. (10a) is replaced with $\lambda\hat{u}$, where $\lambda=-i\alpha c$ is the growth rate. We also assume that the waves are short, and hence we substitute U' in Eq. (10a) with $-r$, as short waves do not "feel" the profile of the basic flow.

Short neutral waves ($\lambda=0$) then are described by

$$\hat{v}^{IV}-2\alpha^2\hat{v}''+\alpha^4\hat{v}=i\alpha\,\mathrm{Re}\,r\hat{v}', \tag{42}$$

the corresponding equation to (31a) for longitudinal rolls. All other equations for longitudinal rolls, (31b), (31c), (32), and (33), remain the same if we replace β with α. Hence, the only difference between the former case and transverse rolls, is the term on the right-hand side of (42). The significance of this term is that now our perturbations are traveling waves (which are not steady, even in the frame moving with the surface velocity). Alternatively, transverse rolls can be obtained from Eqs. (14)–(16) by setting $\hat{h}=0$, $U\sim(3/2)-r$, and $U'\sim -r$, but the resulting system is more involved than (42) and (31b), (31c), (32), and (33).

For $\alpha\,\mathrm{Re}\ll 1$, so that Re must be sufficiently small for the waves to be short (in this limit convective rolls along the transverse direction are driven mainly by the Marangoni effect), we can neglect the term on the right-hand side of (42) and hence we expect for the neutral wavenumber α_0 the same results with β_0 for longitudinal rolls. We could then use (37) for longitudinal perturbations to describe transverse ones (Pr now must be sufficiently large for $\mathrm{Re}\,\mathrm{Pr}\gg 1$). The only difference is that the rolls now are not steady, but they travel with a certain velocity: the correction term on the right-hand side of (42) is mainly responsible for the velocity of the waves, so that λ is not real anymore, but it has an imaginary part.

In fact, using a perturbation expansion with $\alpha\,\mathrm{Re}\ll 1$, it can be shown that transverse rolls have a phase velocity slightly below $3/2-r$, and hence they lag behind the free surface. This also means that the velocity depends on the wavenumber and therefore for long waves the results will be very different. Numerical analysis of the full problem confirms that, indeed, transverse rolls travel with velocity that depends on their wavenumber, while for large values of α their velocity is indeed close to the surface velocity.

V. NUMERICAL ANALYSIS FOR TRANSVERSE WAVES

For arbitrary values of the parameters we must resort to a numerical solution of the full problem. Here we focus on transverse waves. Let us take an initial guess for the eigenvalue, $c=c(0)$. The velocity field can be obtained from (14a) and prior to solving the heat transport problem, as the conditions (15a) and (15c) and the first two conditions in (16) do not depend on the temperature field. Taking into account (16), we seek ϕ in the form

$$\phi = A_1\phi_1 + A_2\phi_2, \tag{43a}$$

where $A_{1,2}$ are unknown at this stage and $\phi_{1,2}$ are solutions of (14a) satisfying at $y=0$ the conditions

$$\phi_1=\phi_1'=\phi_1''=0, \quad \phi_1'''=1, \tag{43b}$$

$$\phi_2=\phi_2'=\phi_2'''=0, \quad \phi_2''=1. \tag{43c}$$

The Orr-Sommerfeld equation is then numerically integrated twice with these boundary conditions to obtain $\phi_{1,2}$. The constants $A_{1,2}$ are obtained by applying conditions (15a) and (15c). Once ϕ is known, we consider the heat transport problem. $\hat{\theta}$ is sought in the form

$$\hat{\theta} = \hat{\theta}_* + B_1 \hat{\theta}_1, \tag{44a}$$

where $\hat{\theta}_*$ and $\hat{\theta}_1$ satisfy at $y=0$ the conditions

$$\hat{\theta}_* = \hat{\theta}_*' = 0, \quad \hat{\theta}_1 = 0, \quad \hat{\theta}_1' = 1. \tag{44b}$$

To obtain $\hat{\theta}_*$, the energy equation (14b) is numerically integrated twice from $y=0$ to $y=1$ with the conditions (44b). For the $\hat{\theta}_1$ integration we assume $\phi=0$. The constant B_1 is then obtained from (15b). The boundary condition (15d) has not been used yet. It is now used to obtain a new approximation for the eigenvalue $c=c^{(n)}$, $n=1$. The whole process is repeated until the required accuracy is satisfied.

Results of the numerical analysis for the neutral wavenumber α_0 as a function of the parameter r are presented in Fig. 6 for a vertical plane, $\theta=\pi/2$, with $\Gamma=2850$ and $\mathrm{Pr}=7$ (water at 25°). In all cases instability occurs below the neutral curve and stability above. First of all, the numerical scheme confirms the main result of the long-wave analysis in Sec. III: in all cases, and as r increases, the thermocapillary forces first destabilize the flow, later on stabilize it, and eventually completely suppress the instability. The analytically predicted value in Sec. III, $r_0=2.52$ for water at 25°, is in excellent agreement with the computations.

For the relatively small value of the Reynolds number $\mathrm{Re}=1$ in Fig. 6(a), the analytical prediction for long surface waves in Eq. (23) agrees very well with the numerical result over the whole range of unstable r. With increasing the Reynolds number to $\mathrm{Re}=5$, we note a deviation between the analytical prediction and the numerically obtained neutral curve inside the unstable region predicted analytically: the exact neutral curve is below the analytically predicted one so that the instability region shrinks and the Marangoni forces have a stabilizing influence. The deviation is simply due to the fact that as Re increases, the term $\mathrm{Re}^3[a_4 r^4 + a_5 r^3 - a_6 r^2 - a_7 r - (75872/25025)] - \mathrm{Re}[a_8 r^2 - a_9 r - (1413/224)]$, in (21d) is no longer negligible compared to $\mathrm{We}\,\mathrm{Re}/3$, and the full expression for c_3 must be utilized.

For $\mathrm{Re} \geqslant 3$ there appears a second region of instability associated with the onset generation of convective rolls. This second branch is shown in Fig. 6(c) for $\mathrm{Re}=10$ [upper dashed line; the lower dashed line corresponds to long surface waves in (23)]. It is obtained from Eq. (37a) with $\beta_0 \to \alpha_0$ (also see the discussion in Sec. IV). Hence, this branch represents short convective rolls with large α_0. The system bifurcates to convective rolls at $\mathrm{Re}=3$ at which value this second instability region is simply a point. With increasing Re the instability region associated with convective rolls is a closed curve that gradually occupies a larger domain of the stability map (only the upper part of this closed curve is shown here—see Fig. 4 for the lower part). Eventually, the instability region for convective rolls collides with the instability region for surface waves and finally overlaps with a major part of this region (recall that r_2 is close to r_0).

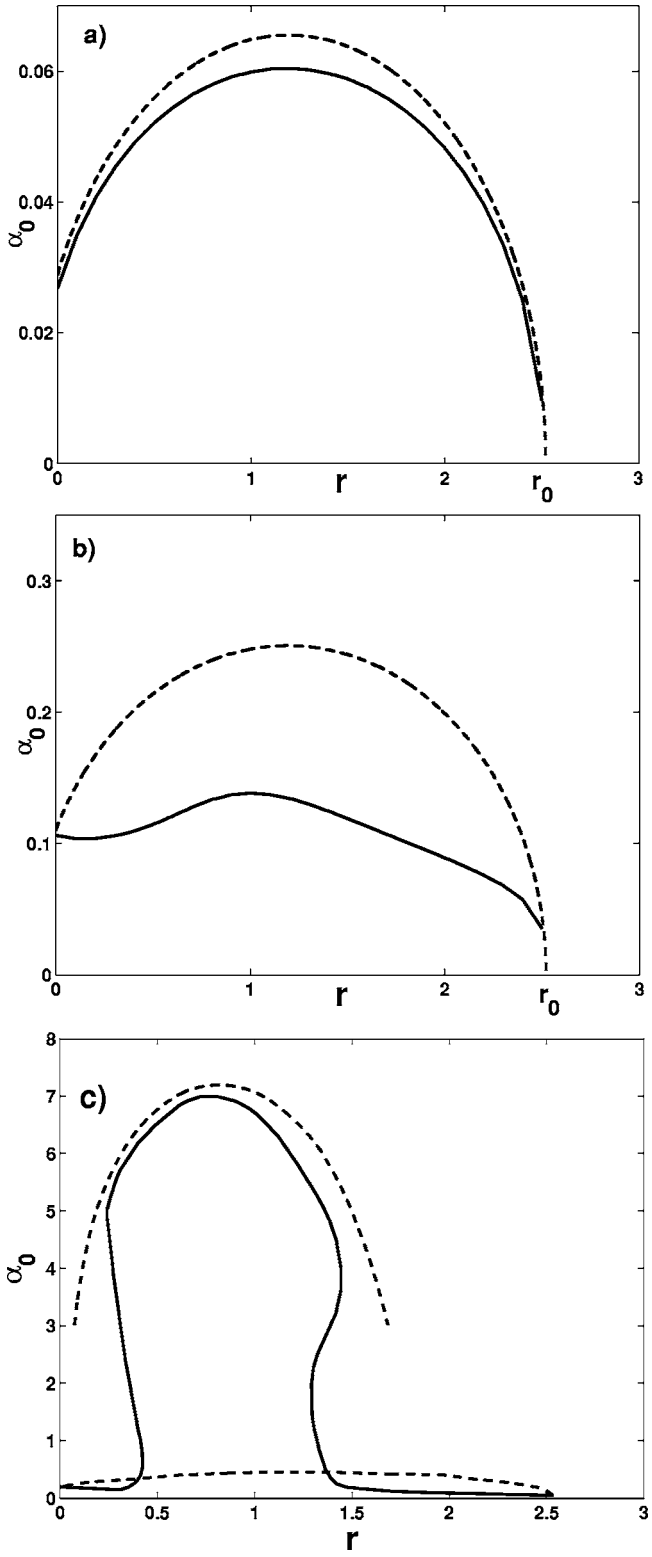

FIG. 6. Neutral stability curves $\alpha_0(r)$ obtained numerically (solid line) from the full system in (14)–(16) for a vertical plane, $\theta=\pi/2$, with $Pr=7$ and $\Gamma=2850$ (water at 25°) and different Reynolds numbers; (a) $\mathrm{Re}=1$. Dashed line: analytical prediction in (23); (b) $\mathrm{Re}=5$. Dashed line: analytical prediction in (23); (c) $\mathrm{Re}=10$. Lower dashed line: analytical prediction in (23). Upper dashed line: convective rolls branch obtained analytically from (37a).

We note that the analytical prediction for convective rolls fits well the numerical results, except for the lower por-

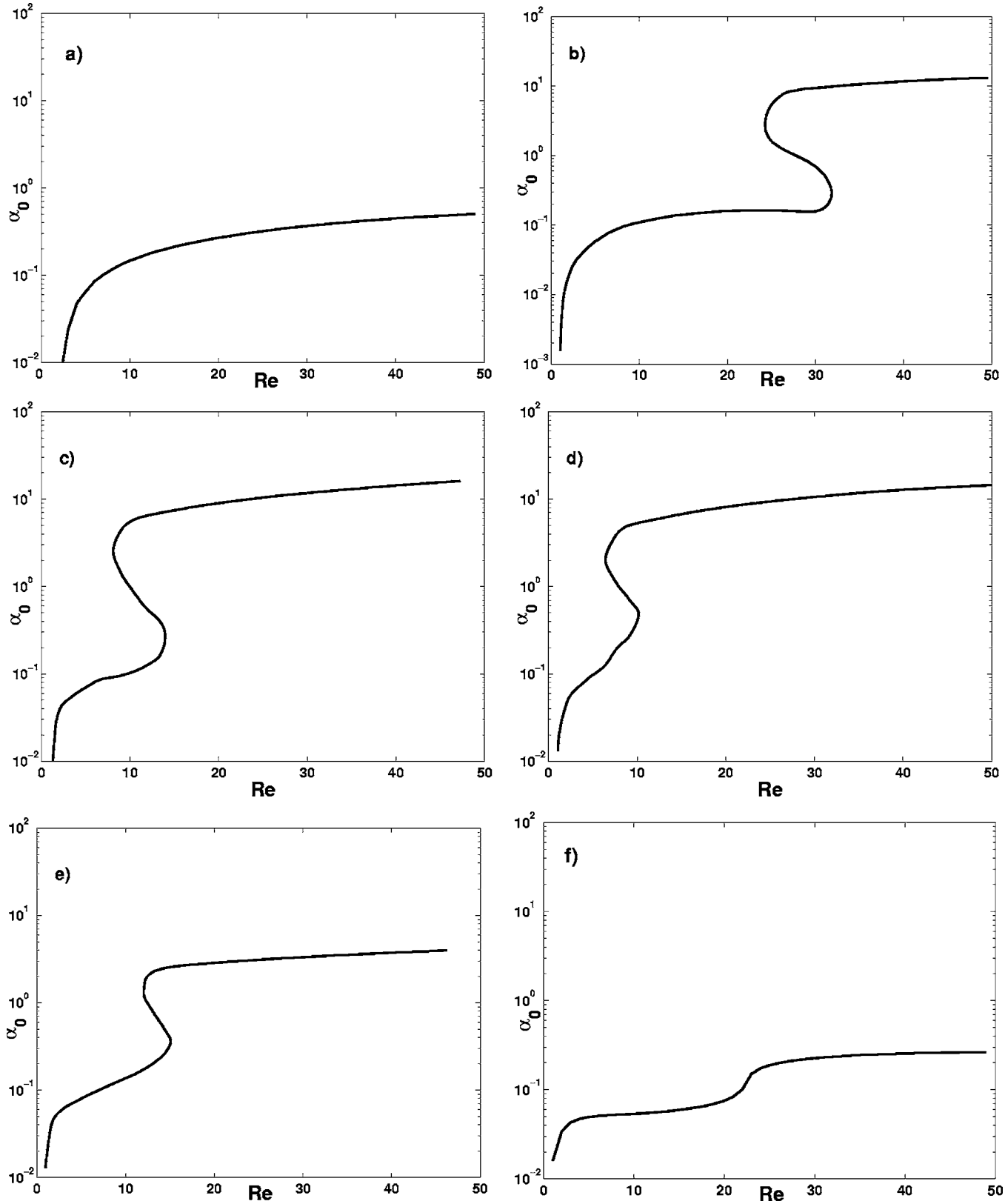

FIG. 7. Neutral stability curves $\alpha_0(\mathrm{Re})$ obtained numerically from the full system in (14)–(16) for a vertical plane, $\theta=\pi/2$, with Pr=7 and $\Gamma=2850$ (water at 25°) and different r; (a) $r=0$; (b) $r=0.2$; (c) $r=0.4$; (d) $r=1.0$; (e) $r=1.5$; (f) $r=2.4$. The lower branch in (b)–(f) corresponds to the surface wave instability and the upper branch to convective rolls.

tion of the neutral curve. On the other hand, the analytical prediction for the neutral curve obtained by assuming long transverse surface waves performs well close to criticality [from (24) for $\theta=\pi/2$, $\mathrm{Re}_*=0$], as shown in Fig. 6(a), but it breaks down further from criticality, as is evident from Figs. 6(b) and 6(c) (also see our discussion in Sec. III). Nevertheless, the long-wave theory seems to perform well in the regions $r\sim 0$ and $r\sim r_0$.

It is also instructive to present the neutral wavenumber as a function of Reynolds number for different values of r, as shown in Fig. 7. In all cases instability occurs below the neutral curve and stability above. For $r=0$ we have the usual surface hydrodynamic instability in the absence of Marangoni effects [Fig. 7(a)]. With increasing temperature gradient convective rolls appear and at some secondary critical Reynolds number they merge with the surface instability region, as discussed earlier. With increasing r the value of the Reynolds number where merging of the two regions occurs decreases [Figs. 7(c) and 7(d)]. Note that as r increases in Figs. 7(a)–7(d) the instability region is enlarged. However, after a certain value of r, which is in good agreement with the value $r_m=1.2$ obtained from (26a), the thermocapillary forces play a stabilizing role [Figs. 7(e) and 7(f)], and for $r > r_0$ the system remains stable for all Re, in agreement also with Fig. 2. However, let us recall the definition of r, $r=3/\mathrm{Bo}$ and the definition of Bo, $\mathrm{Bo}=\rho g h_0 \sin\theta/(\kappa\gamma)$, where $h_0=[3\nu^2\,\mathrm{Re}/(g\sin\theta)]^{1/3}$. It is then clear that small film thicknesses and hence small Re, lead to small values of Bo and hence large values of r, and the condition $r>r_0$ can be easily achieved in the region of small Re. On the other hand, as Re increases, Bo increases, and r decreases, unless of course we increase γ to compensate for large Re and maintain $r>r_0$. Eventually, for very large Re, γ has to be very large also. In this region, it is quite likely that our model will break down as large wall temperature gradients will cause a series of effects (such as density variations, evaporation, etc.) not taken into account by the model.

VI. SUMMARY

We have examined the problem of a film falling down an inclined plane heated with a downward linearly increasing temperature distribution. We have shown that the system is governed by five independent parameters but for given liquid properties and fixed inclination angle, the number of pertinent parameters can be reduced by two, namely, the Reynolds number Re and the dynamic Bond number Bo (an inverse Marangoni number).

The coupled Navier-Stokes and energy equations and associated boundary conditions were linearized to obtain the Orr-Sommerfeld eigenvalue problem for the velocity of the disturbances. We have analyzed the Orr-Sommerfeld problem via appropriate asymptotic and numerical methods. We demonstrated that the instability consists of long-wave surface transverse waves and convective rolls, both transverse and longitudinal. These modes arise from a confrontation between the Kapitza hydrodynamic mode of instability of a free-falling film and the Marangoni instability driven by the thermocapillary stresses on the interface. This competition is monitored by the two Reynolds numbers in the system, Re and Pe.

With respect to surface transverse disturbances, we have performed a perturbation expansion of the Orr-Sommerfeld/linearized energy equations by taking the disturbance wavenumber to be small. We obtained the dispersion relation for long surface waves in closed form and we demonstrated that in contrast to the case of a film falling down a uniformly heated wall, where the Marangoni effect reduces the critical Reynolds number for the instability onset and hence has a destabilizing influence, in our case the thermocapillary forces can either stabilize or destabilize the flow. For a value of Pr larger than $8/25$, as r increases the critical Reynolds number for the onset of the instability decreases (the larger the Pr, the stronger such destabilizing effect) up to a certain r, above which it increases (at this value of r the critical Reynolds for water with $\mathrm{Pr}=7$ decreases five times compared to that for an isothermal film). On the other hand, for $\mathrm{Pr} < 8/25$ the critical Reynolds number for the instability onset increases monotonically and hence the Marangoni forces induce a monotonic stabilization. Eventually, at some value of r that depends weakly on Pr the instability is completely suppressed.

Unlike surface transverse waves that are a long-wave variety, convective rolls, both transverse and longitudinal, were shown to appear from both long-wave and short-wave instabilities. For these modes, surface deformation is negligible. Longitudinal rolls are stationary and they exhibit two critical values of r so that the instability occurs within a finite region $r_1<r<r_2$, which grows as Re increases, but the boundaries r_1 and r_2 remain practically unaltered. The same instability region applies for transverse rolls, however, unlike longitudinal rolls they are not stationary but they travel with a velocity close to the surface velocity of the plane parallel flow.

Finally, numerical computations of the full eigenvalue problem confirmed our approximate analytical predictions. For sufficiently small r we have the usual surface wave instability of a free-falling falling film. With increasing r convective rolls appear also and at some critical Reynolds number they merge with the surface instability region. In the meantime the instability region grows, in fact the Marangoni stresses produce a strong instability with a band of unstable wavenumbers covering a region from zero to ten. However, after a critical value of r the thermocapillary forces play a stabilizing role and eventually suppress all instabilities, leading to a waveless flow regime.

ACKNOWLEDGMENTS

We are grateful to the anonymous referees for useful comments and suggestions. We are also grateful to Dr. C. Ruyer-Quil, Dr. B. Scheid, Dr. P. M. J. Trevelyan and to Professor R. Kh. Zeytounian for numerous stimulating discussions. We thank Nikolay Saprykin and Sergey Saprykin for assistance with the computations in Figs. 5–7. E.A.D. and S.K. thank the Instituto Pluridisciplinar for hospitality and acknowledge financial support from the Spanish Ministry of Science and Technology under Grant No. PB 96-599. E.A.D. also benefited from financial support through the Spanish Ministry of Education and Culture and S.K. through an EPSRC Advanced Fellowship, Grant No. GR/S49520/01.

APPENDIX: SOLUTION OF THE EIGENVALUE PROBLEM IN (28)–(30)

Combining (28b), (28c), and (28e) gives

$$\hat{v}'''' - 2\beta^2\hat{v}'' + \beta^4\hat{v} = \mathrm{Re}\,\lambda(\hat{v}'' - \beta^2\hat{v}), \tag{A1a}$$

with characteristic equation $(\delta^2-\beta^2)^2=\mathrm{Re}\,\lambda(\delta^2-\beta^2)$ with roots $\delta_{1,2}=\pm\beta$ and $\delta_{3,4}=\pm\sqrt{\beta^2+\mathrm{Re}\,\lambda}\equiv\pm\zeta$. The general solution of (A1a) is therefore given by

$$\hat{v} = A_1\sinh\beta y + A_2\cosh\beta y + A_3\sinh\zeta y + A_4\cosh\zeta y. \tag{A1b}$$

From (29a) $A_4=-A_2$ while (28e) and (30) imply $\hat{v}'=0$ at $y=0$, which gives $\beta A_1+\zeta A_3=0$. The solution for $\hat{v}$ can then be written as

$$\hat{v} = \frac{\mathcal{A}}{\beta}\sinh\beta y + \mathcal{B}\cosh\beta y - \frac{\mathcal{A}}{\zeta}\sinh\zeta y - \mathcal{B}\cosh\zeta y, \tag{A1c}$$

where $\mathcal{A}=\beta A_1$ and $\mathcal{B}=A_2$. Applying now (29a) gives

$$\mathcal{A}\left(\frac{\sinh\beta}{\beta} - \frac{\sinh\zeta}{\zeta}\right) = \mathcal{B}(\cosh\zeta - \cosh\beta).$$

However, one of the coefficients $\mathcal{A}$, $\mathcal{B}$ is arbitrary. Let us then without loss of generality set $\mathcal{B}=1$. Equation (A1c) is then written as

$$\hat{v} = \frac{\mathcal{A}}{\beta}\sinh\beta y - \frac{\mathcal{A}}{\zeta}\sinh\zeta y + \cosh\beta y - \cosh\zeta y, \tag{A2a}$$

where

$$\mathcal{A} = \frac{\cosh\zeta - \cosh\beta}{\frac{1}{\beta}\sinh\beta - \frac{1}{\zeta}\sinh\zeta}. \tag{A2b}$$

Equation (28a) can now be written as

$$\hat{u}'' - \xi^2\hat{u} = \mathrm{Re}(3 - r - 3y)\hat{v}, \tag{A3a}$$

the general solution of which is

$$\begin{aligned}\hat{u} = {} & \mathcal{E}\sinh\zeta y + \left(-\mathcal{A}\frac{3\,\mathrm{Re}}{4\zeta^3} - \frac{\mathrm{Re}(3-r)}{2\zeta}\right)y\sinh\zeta y \\ & + \frac{3\,\mathrm{Re}}{4\zeta}y^2\sinh\zeta y + \mathcal{M}\cosh\zeta y + \left(-\mathcal{A}\frac{\mathrm{Re}(3-r)}{2\zeta^2} \right. \\ & \left. - \frac{3\,\mathrm{Re}}{4\zeta^2}\right)y\cosh\zeta y + \mathcal{A}\frac{3\,\mathrm{Re}}{4\zeta^2}y^2\cosh\zeta y + \left(\frac{6\beta}{\mathrm{Re}\,\lambda^2} \right. \\ & \left. - \mathcal{A}\frac{(3-r)}{\lambda\beta}\right)\sinh\beta y + \frac{3\mathcal{A}}{\beta\lambda}y\sinh\beta y + \left(\frac{6\mathcal{A}}{\mathrm{Re}\,\lambda^2} \right. \\ & \left. - \frac{(3-r)}{\lambda}\right)\cosh\beta y + \frac{3}{\lambda}y\cosh\beta y, \end{aligned} \tag{A3b}$$

which is a sum of the general solution of the corresponding homogeneous equation and a particular solution of the nonhomogeneous equation (obtained by using the method of variation of parameters). Applying (30) now gives

$$\mathcal{M} = -\frac{6\mathcal{A}}{\mathrm{Re}\,\lambda^2} + \frac{(3-r)}{\lambda}, \tag{A3c}$$

where $\mathcal{A}$ is given by (A2b). $\mathcal{E}$ can then be obtained from (29b):

$$\begin{aligned}\mathcal{E} = {} & \left(\mathcal{A}\frac{3\,\mathrm{Re}}{4\zeta^4} + \frac{\mathrm{Re}(3-r)}{2\zeta^2}\right)(\zeta + \tanh\zeta) - \frac{3\,\mathrm{Re}}{4\zeta^2}(\zeta \\ & + 2\tanh\zeta) + \left(\frac{6\mathcal{A}}{\mathrm{Re}\,\lambda^2} - \frac{(3-r)}{\lambda}\right)\tanh\zeta \\ & + \left(\mathcal{A}\frac{\mathrm{Re}(3-r)}{2\zeta^3} + \frac{3\,\mathrm{Re}}{4\zeta^3}\right)(1 + \zeta\tanh\zeta) - \mathcal{A}\frac{3\,\mathrm{Re}}{4\zeta^3}(2 \\ & + \zeta\tanh\zeta) + \left(-\frac{6\beta}{\mathrm{Re}\,\zeta\lambda^2} + \mathcal{A}\frac{(3-r)}{\lambda\zeta\beta}\right)\beta\frac{\cosh\beta}{\cosh\zeta} \\ & - \frac{3\mathcal{A}}{\beta\lambda\zeta}\left(\frac{\sinh\beta}{\cosh\zeta} + \beta\frac{\cosh\beta}{\cosh\zeta}\right) + \left(-\frac{6\mathcal{A}}{\mathrm{Re}\,\zeta\lambda^2} \right. \\ & \left. + \frac{(3-r)}{\zeta\lambda}\right)\beta\frac{\sinh\beta}{\cosh\zeta} - \frac{3}{\zeta\lambda}\left(\frac{\cosh\beta}{\cosh\zeta} + \beta\frac{\sinh\beta}{\cosh\zeta}\right). \end{aligned} \tag{A3d}$$

We now turn to the linearized energy equation in (28d) that can be written as

$$\hat{\theta}'' - \xi^2\hat{\theta} = \mathrm{Pe}(\hat{u} + \Theta'\hat{v}), \tag{A4a}$$

where $\xi^2=\beta^2+\lambda\,\mathrm{Pe}$ and

$$\begin{aligned}\hat{u} + \Theta'\hat{v} = {} & (\mathcal{A}_1 + \mathcal{A}_2 y + \mathcal{A}_3 y^2 + \mathcal{A}_4 y^3)\sinh\zeta y + (\mathcal{B}_1 + \mathcal{B}_2 y \\ & + \mathcal{B}_3 y^2 + \mathcal{B}_4 y^3)\cosh\zeta y + (\mathcal{E}_1 + \mathcal{E}_2 y + \mathcal{E}_3 y^2 \\ & + \mathcal{E}_4 y^3)\sinh\beta y + (\mathcal{D}_1 + \mathcal{D}_2 y + \mathcal{D}_3 y^2 \\ & + \mathcal{D}_4 y^3)\cosh\beta y. \end{aligned} \tag{A4b}$$

The different constants are given by

$$\mathcal{A}_1 = \mathcal{E} - \mathcal{A}\frac{\mathrm{Pe}\left(\frac{1}{2}r - 1\right)}{\zeta},$$

$$\mathcal{A}_2 = -\mathcal{A}\frac{3\,\mathrm{Re}}{4\zeta^3} - \frac{\mathrm{Re}(3-r)}{2\zeta} - \mathcal{A}\frac{\mathrm{Pe}\left(\frac{3}{2} - \frac{1}{2}r\right)}{\zeta},$$

$$\mathcal{A}_3 = \frac{3\,\mathrm{Re}}{4\zeta}, \quad \mathcal{A}_4 = \mathcal{A}\frac{\mathrm{Pe}}{2\zeta},$$

$$\mathcal{B}_1 = \mathcal{M} - \mathrm{Pe}\left(\frac{1}{2}r - 1\right),$$

$$\mathcal{B}_2 = -\mathcal{A}\frac{\mathrm{Re}(3-r)}{2\zeta^2} - \frac{3\,\mathrm{Re}}{4\zeta^2} - \mathrm{Pe}\left(\frac{3}{2} - \frac{1}{2}r\right),$$

$$\mathcal{B}_3 = \mathcal{A}\frac{3\,\mathrm{Re}}{4\zeta^2}, \quad \mathcal{B}_4 = \frac{1}{2}\,\mathrm{Pe},$$

$$\mathcal{E}_1 = \frac{6\beta}{\mathrm{Re}\,\lambda^2} - \mathcal{A}\frac{(3-r)}{\lambda\beta} + \mathcal{A}\frac{\mathrm{Pe}\left(\frac{1}{2}r-1\right)}{\beta}, \quad \mathcal{E}_2 = \frac{3\mathcal{A}}{\beta\lambda},$$

$$\mathcal{E}_3 = \mathcal{A}\frac{\mathrm{Pe}\left(\frac{3}{2}-\frac{1}{2}r\right)}{\beta}, \quad \mathcal{E}_4 = -\mathcal{A}\frac{\mathrm{Pe}}{2\beta},$$

and

$$\mathcal{D}_1 = \frac{6\mathcal{A}}{\mathrm{Re}\,\lambda^2} - \frac{(3-r)}{\lambda} + \mathrm{Pe}\left(\frac{1}{2}r-1\right), \quad \mathcal{D}_2 = \frac{3}{\lambda},$$

$$\mathcal{D}_3 = \mathrm{Pe}\left(\frac{3}{2}-\frac{1}{2}r\right), \quad \mathcal{D}_4 = -\frac{1}{2}\mathrm{Pe}.$$

The general solution of (A4a) is

$$\hat{\theta} = \mathcal{L}\sinh\xi y + \mathcal{K}\cosh\xi y + \hat{\theta}^*, \tag{A4c}$$

with $\hat{\theta}^*$ a particular solution that is rather lengthy and is not given here. Applying (30) gives

$$\mathcal{K} = -\hat{\theta}^*(0) \tag{A4d}$$

while (29d) gives

$$\mathcal{L} = -\mathcal{K}\tanh\xi - \frac{\hat{\theta}^{*\prime}(1)}{\xi\cosh\xi}. \tag{A4e}$$

Substituting then $\hat{\theta}$ into (29c) gives the dispersion relation. Here (29c) originates from the tangential stress balance in (11c) and the continuity equation in (28e). Hence, like the case of transverse instabilities and surface waves analyzed in Sec. III, the eigenvalue for longitudinal rolls is effectively determined by the Marangoni forces.

The final form of the dispersion relation is rather lengthy and cumbersome and is not given here. A numerical analysis of the dispersion relation indicates that λ is real so that $c_r = 0$ and the longitudinal rolls are standing waves.

[1] A. A. Nepomnyashchy, M. G. Velarde, and P. Colinet, *Interfacial Phenomena and Convection* (Chapman & Hall, London, 2002).
[2] M. K. Chaudhury and G. M. Whitesides, "How to make water run uphill," Science **256**, 1539 (1992).
[3] R. Vuilleumier, V. Ego, L. Neltner, and A. M. Cazabat, "Tears of wine: the stationary state," Langmuir **11**, 4117 (1995).
[4] J. R. A. Pearson, "On convection cells induced by surface tension," J. Fluid Mech. **4**, 21 (1958).
[5] L. E. Scriven and C. Sternling, "On cellular convection driven by surface-tension gradients: effects of mean surface tension and surface viscosity," J. Fluid Mech. **19**, 321 (1964).
[6] M. G. Velarde, A. A. Nepomnyashchy, and M. Hennenberg, "Onset of oscillatory interfacial instability and wave motions in Benárd layers," Adv. Appl. Mech. **37**, 167 (2000).
[7] K. A. Smith, "On convective instability induced by surface-tension gradients," J. Fluid Mech. **24**, 401 (1966).
[8] D. A. Goussis and R. E. Kelly, "On the thermocapillary instabilities in a liquid layer heated from below," Int. J. Heat Mass Transfer **33**, 2237 (1990).
[9] M. K. Smith and S. H. Davis, "Instabilities of dynamic thermocapillary liquid layers. Part 1. Convective instabilities," J. Fluid Mech. **132**, 119 (1983).
[10] M. K. Smith and S. H. Davis, "Instabilities of dynamic thermocapillary liquid layers. Part 2. Surface-wave instabilities," J. Fluid Mech. **132**, 145 (1983).
[11] S. H. Davis, "Thermocapillary instabilities," Annu. Rev. Fluid Mech. **19**, 403 (1987).
[12] V. M. Shevtsova, A. A. Nepomnyashchy, and J. C. Legros, "Thermocapillary-buoyancy convection in a shallow cavity heated from the side," Phys. Rev. E **67**, 066308 (2003).
[13] P. Colinet, J. C. Legros, and M. G. Velarde, *Nonlinear Dynamics of Surface-Tension-Driven Instabilities* (Wiley-VCH, Berlin, 2001).
[14] *Interfacial Phenomena and the Marangoni Effect*, edited by M. G. Velarde and R. Kh. Zeytounian (Springer-Verlag, New York, 2002).
[15] D. A. Goussis and R. E. Kelly, "Surface waves and thermocapillary instabilities in a liquid film flow," J. Fluid Mech. **223**, 25 (1991).
[16] P. L. Kapitza, "Wave flow of thin viscous fluid layers," Zh. Eksp. Teor. Fiz. **18**, 1 (1948).
[17] S. G. Bankoff, "Stability of liquid flow down a heated inclined plane," Int. J. Heat Mass Transfer **14**, 377 (1971).
[18] S. W. Joo, S. H. Davis, and S. G. Bankoff, "Long-wave instabilities of heated falling films: two-dimensional theory of uniform layers," J. Fluid Mech. **230**, 117 (1991).
[19] S. Kalliadasis, E. A. Demekhin, C. Ruyer-Quil, and M. G. Velarde, "Thermocapillary instability and wave formation on a film falling down a uniformly heated plane," J. Fluid Mech. **492**, 303 (2003).
[20] S. Kalliadasis, A. Kiyashko, and E. A. Demekhin, "Marangoni instability of a thin liquid film heated from below by a local heat source," J. Fluid Mech. **475**, 377 (2003).
[21] V. Ya. Shkadov, "Wave modes in the flow of thin layer of a viscous liquid under the action of gravity," Izv. Akad. Nauk SSSR, Mekh. Zhidk. Gaza **1**, 43 (1967).
[22] V. Ya. Shkadov, "Theory of wave flow of a thin layer of a viscous liquid," Izv. Akad. Nauk SSSR, Mekh. Zhidk. Gaza **2**, 20 (1968).
[23] C. Ruyer-Quil and P. Manneville, "Further accuracy and convergence results on the modeling of flows down inclined planes by weighted-residual approximations," Phys. Fluids **14**, 170 (2002).
[24] P. M. J. Trevelyan and S. Kalliadasis, "Wave dynamics on a thin-liquid film falling down a heated wall," J. Eng. Math. **50**, 177 (2004).
[25] C. Ruyer-Quil, B. Scheid, S. Kalliadasis, M. G. Velarde, and R. Kh. Zeytounian, "Thermocapillary long waves in a liquid film flow. Part 1. Low-dimensional formulation," J. Fluid Mech. **538**, 199 (2005).
[26] B. Scheid, C. Ruyer Quil, S. Kalliadasis, M. G. Velarde, and R. Kh. Zeytounian, "Thermocapillary long waves in a liquid film flow. Part 2. Linear stability and nonlinear waves," J. Fluid Mech. **538**, 223 (2005).
[27] V. Ya. Shkadov, M. G. Velarde, and V. P. Shkadova, "Falling films and the Marangoni effect," Phys. Rev. E **69**, 056310 (2004).
[28] P. M. J. Trevelyan and S. Kalliadasis, "Dynamics of a reactive falling film at large Péclet numbers. I. Long-wave approximation," Phys. Fluids **16**, 3191 (2004).
[29] P. M. J. Trevelyan and S. Kalliadasis, "Dynamics of a reactive falling film at large Péclet numbers. II. Nonlinear waves far from criticality: Integral-boundary-layer approximation," Phys. Fluids **16**, 3209 (2004).
[30] V. Ludviksson and E. N. Lightfoot, "Hydrodynamic stability of Marangoni films," AIChE J. **14**, 621 (1968).
[31] S. Miladinova, S. Slavtchev, G. Lebon, and J.-C. Legros, "Long-wave instabilities of non-uniformly heated falling films," J. Fluid Mech. **453**, 153 (2002).
[32] S. Miladinova, D. Staykova, G. Lebon, and B. Scheid, "Effect of nonuniform wall heating on the three-dimensional instability of falling films," Acta Mech. **156**, 79 (2002).
[33] L. G. Leal, *Laminar Flow and Convective Transport Processes* (Butterworth-Heinemann, Newton, MA, 1992).
[34] R. Aris, *Vectors, Tensors, and the Basic Equations of Fluid Mechanics* (Dover, New York, 1962).
[35] T. B. Benjamin, "Wave formation in laminar flow down an inclined plane," J. Fluid Mech. **2**, 554 (1971).
[36] C.-S. Yih, "Stability of liquid flow down an inclined plane," Phys. Fluids **6**, 321 (1963).
[37] H.-C. Chang, "Wave evolution on a falling film," Annu. Rev. Fluid Mech. **26**, 103 (1994).
[38] H.-C. Chang and E. A. Demekhin, *Complex Wave Dynamics in Thin Films* (Elsevier Scientific, Amsterdam, 2002).
[39] A. Ye. Rednikov, P. Colinet, M. G. Velarde, and J. C. Legros, "Rayleigh-Marangoni oscillatory instability in a horizontal liquid layer heated from above: coupling and mode mixing of internal and surface dilational waves," J. Fluid Mech. **45**, 57 (2000).